# Electronic energy-band structure of the calcium fluoride crystal

Richard A. Heaton and Chun C. Lin
*Department of Physics, University of Wisconsin, Madison, Wisconsin 53706*
(Received 12 May 1980)

A self-consistent-field calculation for the electronic energy-band structure of the $CaF_2$ crystal has been performed by using the method of linear combinations of atomic orbitals. The basis set consists of 90 Bloch sums formed by atomic wave functions of Ca and F as well as single-Gaussian orbitals. The valence-band states are composed chiefly of F $2p$ orbitals with both the upper and lower edges at the $X$ point. The x-ray structure factors are obtained from the valence-band wave functions and are compared with the observed values. The conduction states in the energy range of 1–3 eV above the threshold have substantial admixture of the Ca $3d$ orbitals, resulting in high density of states in that region. The calculated band gap is 10.0 eV which is somewhat smaller than the experimental value estimated from the reflectance spectra. Comparison of the calculated joint density of states with experimental optical data is discussed.

## I. INTRODUCTION

The alkaline earth fluoride crystals have attracted considerable attention because of their wide band gap and their roles as host crystals for doped impurities. For the case of $CaF_2$ optical measurements in the ultraviolet region have been reported by several research groups.[1-5] Considerable disagreement exists in the literature concerning the interpretation of the optical data, because empirical energy-band structures were assumed in order to assign the observed structure to interband transitions. Recently Albert, Jouanin, and Gout have performed first-principles calculations of the band structure of $CaF_2$.[6] They used the method of linear combinations of atomic orbitals (LCAO) for the valence band (VB) and the method of orthogonalized plane waves (OPW) for the conduction bands (CB). Because of the slow convergence of the OPW expansion for $d$ states, their calculated energies for the $\Gamma_{12}$ and $\Gamma'_{25}$ CB states are too high. Albert *et al.* subsequently recalculated the CB using the pseudopotential method, but the $d$-like states still remain too high in the CB.[7] To bring these states to the correct proximity, an empirical $l$-dependent potential had to be added. The CB obtained by either version of the pseudopotential method differ significantly from the OPW results. A survey of the earlier energy-band structures based on empirical consideration or more fundamental approaches has been given in Ref. 6. The works of Albert *et al.* represent the most rigorous efforts to that date.

We present in this paper a self-consistent-field calculation for both the VB and CB using the LCAO method. This work differs from that of Albert *et al.* in two major ways. Our basis functions include not only Bloch sums of the occupied states of the $Ca^{++}$ and $F^-$ ions, but also Bloch sums composed of single-Gaussian-type orbitals (GTO) of varying widths located at the cation and anion sites. It has been shown that accurate CB energies can be obtained from the LCAO method if the basis set is augmented to include single-Gaussian Bloch sums.[8] Secondly our energy-band calculation is carried to self-consistency, whereas in Refs. 6 and 7 the crystal potential is approximated by a lattice summation of the individual free-ion potentials with a modification for the exchange term. With the LCAO method no convergence difficulty arises for the $d$ states. Indeed our $\Gamma_{12}$ and $\Gamma'_{25}$ energies lie much lower in the CB as compared to those of Ref. 6. Based on the joint density of states (JDOS) of our calculated VB and CB, we are able to interpret some of the observed optical structures in terms of band-to-band transitions.

## II. ENERGY-BAND CALCULATION

The crystal structure of $CaF_2$ can be thought of as three interpenetrating face-centered-cubic (fcc) lattices of the same lattice constant ($a = 10.32$ a.u.), one consisting entirely of Ca atoms and the other two due to the two sets of F atoms which are not translation-related to each other. Placing the origin at a Ca atom, we write a Bloch-sum basis function for the Ca atom as

$$b_i^{\mathrm{Ca}}(\vec{k},\vec{r}) = \sum_\nu \exp(i\vec{k}\cdot\vec{R}_\nu)\phi_i^{\mathrm{Ca}}(\vec{r}-\vec{R}_\nu)\,, \tag{1}$$

where $\vec{R}_\nu$ represents a translational vector for the fcc lattice, and $\phi_i$ a localized function. Similarly the two Bloch sums associated with the two F sublattices are

$$\begin{aligned} b_j^{\mathrm{F}1}(\vec{k},\vec{r}) &= \sum_\nu \exp(i\vec{k}\cdot\vec{R}_\nu)\phi_j^{\mathrm{F}}(\vec{r}-\vec{t}_1-\vec{R}_\nu)\,, \\ b_j^{\mathrm{F}2}(\vec{k},\vec{r}) &= \sum_\nu \exp(i\vec{k}\cdot\vec{R}_\nu)\phi_j^{\mathrm{F}}(\vec{r}-\vec{t}_2-\vec{R}_\nu)\,, \end{aligned} \tag{2}$$

 

where

$$\vec{t}_1 = -\vec{t}_2 = \tfrac{1}{4}a(1,1,1)\,. \tag{3}$$

In the traditional LCAO approach,[9,10] the localized functions $\phi$ are identified as the wave functions of all the occupied shells of the free atoms, expanded in Gaussian-type orbitals, e.g.,

$$\phi_{ns} = \sum_i a_i \exp(-\beta_i r^2), \text{ etc.} \tag{4}$$

Our Gaussian-basis atomic wave functions for $F^-$ and $Ca^{++}$ are determined by a self-consistent-field (SCF) Hartree-Fock-Slater procedure.[11] For computational efficiency we use, for both F and Ca functions, the same set of Gaussian exponents: $\beta = 25\,873$, 5894.9, 1712.02, 563.304, 204.797, 80.4187, 33.1145, 9.862 21, 3.977 75, 2.691 63, 1.731 93, 0.977 055, 0.620 640, 0.396 147, 0.206 990, 0.10. To attain higher accuracy for the band energies, we use, in addition to the conventional atomic-orbital basis functions, a series of Bloch sums formed by single Gaussians,[8,10] namely, the $\phi$ functions in Eq. (1) are taken as $\exp(-\beta r^2)$, or $x\exp(-\beta r^2)$, etc. For the VB states, a basis set consisting of Bloch sums of atomic orbitals with the option of some single-Gaussian supplement should be quite adequate. To describe the CB the use of single-Gaussian Bloch sums becomes essential in order to represent the diffuse nature of the conduction states.

To obtain a self-consistent-field energy-band structure, we start with a zeroth-order approximation of the crystal electron density which is taken as a superposition of the free-atom electron densities of the $Ca^{++}$ and $F^-$ ions,

$$\rho^{(0)}_{\rm cry}(\vec{r}) = \sum_\nu [\rho_{Ca^{++}}(\vec{r} - \vec{R}_\nu) + \rho_{F^-}(\vec{r} - \vec{t}_1 - \vec{R}_\nu) + \rho_{F^-}(\vec{r} - \vec{t}_2 - \vec{R}_\nu)]\,. \tag{5}$$

The zeroth-order Coulomb part of the crystal potential, $V_C^{(0)}$, can then be obtained by direct integration. The exchange part is given by the standard statistical approximation

$$V_X = -\tfrac{3}{2}\alpha[3\rho_{\rm cry}(\vec{r})/\pi]^{1/3}\,, \tag{6}$$

with the exchange parameter $\alpha$ set to unity. (Discussion of the choice of $\alpha$ will be given in Sec. V.) Thus we compute the values of $[\rho^{(0)}_{\rm cry}(\vec{r})]^{1/3}$ for a large number of nonequivalent points and curve-fit them to a lattice superposition of some localized functions,

$$[\rho^{(0)}_{\rm cry}(\vec{r})]^{1/3} = \sum_\nu [g_c(\vec{r} - \vec{R}_\nu) + g_a(\vec{r} - \vec{t}_1 - \vec{R}_\nu) + g_a(\vec{r} - \vec{t}_2 - \vec{R}_\nu)]\,, \tag{7}$$

where the subscripts $c$ and $a$ refer to the cations and anions, respectively. The functional forms of $g(\vec{r})$ which we adopt are

$$g_c(\vec{r}) = w_c(r)\,, \tag{8}$$

$$g_a(\vec{r}) = w_a(r) + w_a'(r)xyz\,, \tag{9}$$

where $w_c$, $w_a$, and $w_a'$ are functions of $r$ alone in the general form of

$$\sum_{i,n} a_{in} r^n \exp(-\zeta_i r)\,. \tag{10}$$

The difference in functional form between $g_c$ and $g_a$ is due to the fact that the local symmetry around the cation is octahedral whereas the anions are tetrahedrally coordinated. One could have added a term such as $(x^4 + y^4 + z^4 - \frac{3}{5}r^4)w''(r)$ to both $g_c$ and $g_a$, but this is not necessary since we are able to get a very good fit with Eqs. (8) and (9). With the coordinate origin placed at a Ca site, the crystal potential exhibits inversion symmetry and can be expanded as

$$V_{\rm cry}(\vec{r}) = \sum_\nu V(\vec{K}_\nu)\cos\vec{K}_\nu \cdot \vec{r}\,, \tag{11}$$

where the $\vec{K}_\nu$ vectors span the reciprocal lattice of the fcc system. Our zeroth-order approximation may be referred to as the overlapping-atomic-charge (OAC) model. It differs from the overlapping-atomic-potential (OAP) model in that the OAP exchange potential is obtained by taking the sum of the $\rho^{1/3}$ of the individual atoms rather than the cubic root of the sum of atomic charge density. The OAP model tends to overestimate the exchange term in the region where charge density is very low. We find that the OAC model is closer to the SCF potential than is the OAP. To determine the SCF crystal potential, only a moderate basis-function set is sufficient since the SCF potential is governed entirely by the occupied-state wave functions which retain most of the atomic character. We choose for our basis set a total of 51 functions. They are Bloch sums of $Ca^{++}$ $1s, 2s, 2p, 3s, 3p$ orbitals, $F^-$ $1s, 2s, 2p$ orbitals, single Gaussians at Ca with $\beta = 0.620\,640$, and 0.10 for $s$ type and $\beta = 0.620\,640$ and 0.206 990 for $p$ type, and single Gaussians at F with $\beta = 1.731\,93$, 0.620 640, and 0.10 for $s$ type and $\beta = 1.731\,93$, 0.620 640, and 0.206 990 for $p$ type. The overlap ($S$) and Hamiltonian ($H$) matrix elements are calculated by methods already described in the literature.[10] To speed up convergence of the $K_\nu$ summation in Eq. (11), we employ an Ewald-type procedure which differs substantially from the one in Ref. 10 and is described in the Appendix. We solve the secular equations $|H_{ij} - ES_{ij}| = 0$ to determine the one-electron energies and wave functions for four $\vec{k}$ points in the Brillouin zone (BZ), namely, $\Gamma$, $X$,

$L$, and $W$. The first-order charge density is then obtained from the occupied-state crystal wave functions by performing a numerical integration over BZ using these four points. We compute the charge density and its cubic root at 353 points within the fundamental wedge of the unit cell, and curve-fit them to a superposition of localized functions at each site:

$$\rho_{\rm cry}^{(1)}(\vec{r})=\sum_{\nu}[\rho_c^{(1)}(\vec{r}-\vec{R}_\nu)+\rho_a^{(1)}(\vec{r}-\vec{R}_\nu-\vec{t}_1)+\rho_a^{(1)}(\vec{r}-\vec{R}_\nu-\vec{t}_2)], \tag{12}$$

$$[\rho_{\rm cry}^{(1)}(\vec{r})]^{1/3}=\sum_{\nu}[g_c^{(1)}(\vec{r}-\vec{R}_\nu)+g_a^{(1)}(\vec{r}-\vec{R}_\nu-\vec{t}_1)+g_a^{(1)}(\vec{r}-\vec{R}_\nu-\vec{t}_2)],$$

where the superscript (1) designates first iteration. The functions $\rho$ and $g$ have similar form except that we find it unnecessary to use the $xyz$ term for $\rho_a$. From $\rho^{(1)}$ and $g^{(1)}$, we derive the Fourier coefficients of the improved crystal potential and subsequently a set of improved energies and wave functions (see Appendix). The iteration procedures are repeated until self-consistency is reached. Similar SCF schemes for LCAO band calculations have been published previously.[12-14]

For the CB states, a larger basis set is needed to adequately describe their oscillatory nature. Furthermore the cation $d$ bands play a prominent role because of the close proximity of the atomic Ca $4s$ and $3d$ states. For instance, the bottom of the CB for the CaO crystal is of $X_3$ symmetry which arises from the $d$ orbitals of Ca.[13] To ensure good convergence for the LCAO expansion we determine the energies at the $\Gamma$, $X$, and $L$ points by using a large set (229 functions) which includes (i) Ca $1s, 2s, 2p, 3s, 3p, 3d$ and F $1s, 2s, 2p$ atomic orbitals, (ii) $s$-type single Gaussians on Ca and F with $\beta=33.1145$, 9.862 21, 3.977 75, 2.691 63, 0.977 055, 0.620 640, 0.396 147, 0.10,

TABLE I. SCF electronic energies of the $CaF_2$ crystal in units of eV. The subscripts $v$ and $c$ represent VB and CB, respectively.

| | Energies | | Energies | | Energies |
|---|---|---|---|---|---|
| $\Gamma'_{25v}$ | −13.27 | $X'_{2v}$ | −11.66 | $L_{3v}$ | −12.77 |
| $\Gamma_{15v}$ | −11.85 | $X_{1c}$ | −1.59 | $L_{1v}$ | −12.62 |
| $\Gamma_{1c}$ | −1.86 | $X_{3c}$ | −0.66 | $L'_{2v}$ | −12.56 |
| $\Gamma_{12c}$ | −0.74 | $X_{2c}$ | 0.003 | $L'_{3v}$ | −12.31 |
| $\Gamma'_{25c}$ | 0.57 | $X_{5c}$ | 0.42 | $L_{3c}$ | −0.56 |
| $\Gamma_{15c}$ | 8.02 | $X'_{4c}$ | 3.88 | $L_{1c}$ | −0.44 |
| $X_{1v}$ | −13.67 | $X_{1c}$ | 5.05 | $L_{3c}$ | 0.45 |
| $X'_{5v}$ | −12.95 | $X_{1c}$ | 7.25 | $L'_{2c}$ | 1.67 |
| $X_{5v}$ | −11.92 | $X'_{5c}$ | 7.97 | $L_{1c}$ | 3.89 |

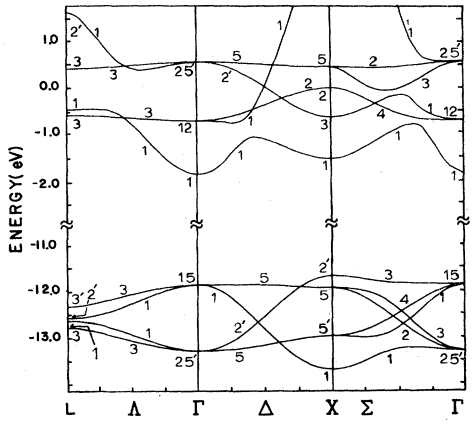


FIG. 1. Valence and conduction bands of $CaF_2$.

(iii) $p$-type single Gaussians on Ca with =3.977 75, 2.691 63, 0.977 055, 0.620 640, 0.396 147, 0.10, and on F with all these $\beta$'s plus $\beta=9.862\,21$, (iv) $d$-type single Gaussians on Ca and F with $\beta=33.1145$, 9.862 21, 3.977 75, 2.691 63, 1.731 93, 0.977 055, 0.620 640, 0.10, and (v) an $s$-type single Gaussian of the form $r^2\exp(-\beta r^2)$ on Ca with $\beta=0.10$. The results are presented in Table I. The energy values given therein are absolute, i.e., $E=0$ corresponds to the vacuum level. A series of test calculations is then performed by deleting a number of single-Gaussian basis functions systematically. Those basis functions which affect the CB states below $\Gamma_{15c}$ by no more than 0.01 a.u. are removed. This leaves us with a set of 77 functions consisting of all the atomic orbitals cited above in (i), two Ca $s$-type single Gaussians ($\beta=0.10$, 0.620 640), two Ca $p$-type ($\beta=0.396\,147$, 0.620 640), two Ca $d$-type ($\beta=0.10$, 0.620 640), three F $s$-type ($\beta=0.10$, 0.620 640, 2.691 63), three F $p$-type ($\beta=0.396\,147$, 0.620 640, 2.691 63), one F $d$-type ($\beta=0.10$), and one Ca $s$-type ($\beta=0.10$) of the form $r^2\exp(-\beta r^2)$. With this basis set we calculate the band structure and the results are shown in Fig. 1. While an extended basis set is essential to obtain accurate CB, there is very little difference in the VB energies between the results of the 77-function set and of the 51-function set which was used to determine the SCF crystal potential.

## III. RESULTS

### A. Valence-band structure

As a qualitative description, the VB of an ionic crystal is usually regarded as being composed of the anion orbitals. In the present case of $CaF_2$, the VB wave functions are overwhelmingly dominated by the F orbitals with only very small contributions from Ca. To obtain a quantitative mea-

sure of Ca admixture, we apply Mulliken's population analysis[15] to the VB wave functions at $\Gamma$, $X$, $L$, and $W$ to determine the fractional charge attributed to the Ca atoms which is found to be less than 0.03 for all 24 states at these four $\vec{k}$ points. As another test for the importance of the Ca contribution to the VB states, we recalculate their energies by dropping from the 51-function basis set all the orbitals centered at the Ca sites except those of the $1s,\ldots,3p$ cores, and find the change in energy less than 0.17 eV at the $\Gamma, X, L, W$ points.

The presence of two F atoms in a unit cell gives rise to two distinct VB levels at the $\Gamma$ point. In Fig. 2(a) we sketch the $p_x$-type orbitals on a layer of F atoms parallel to the $xy$ plane for $\Gamma_{25}'$. The individual atomic orbitals are bonding with respect to the atoms on $x$ axis and antibonding along a line perpendicular to it. Because the orbital overlap is stronger along the $x$ direction, there is a net bonding effect. Conversely, the corresponding state for $\Gamma_{15}$, shown in Fig. 2(b), is antibonding longitudinally and bonding transversely. At the $X$ point a phase reversal occurs between two translation-related atoms whose $x$ coordinates differ by $\frac{1}{2}a$. This transforms Fig. 2 into Fig. 3. The wave function shown in Fig. 3(a) is totally antibonding and 3(b) is totally bonding. For this reason the $X_1$ state lies below $\Gamma_{25}'$, and $X_2'$ lies above $\Gamma_{15}$. In fact the VB edges are at $X$. The presence of Ca orbitals may have some influence on the energies, but this effect is small because of the very low degree of Ca participation in the VB states as discussed in the preceding paragraph.

The calculated density of states (DOS) for the VB is shown in Fig. 4. The two prominent peaks correspond to the states slightly below $\Gamma_{15}$ and those slightly above $\Gamma_{25}'$, whereas the two minor peaks are partly associated with the region near the $L$ point.

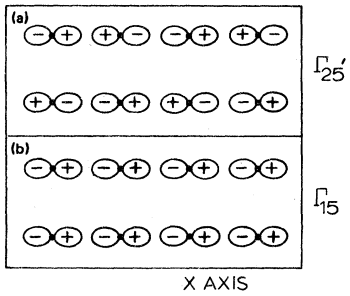


FIG. 2. Schematic diagrams of the $p_x$-type orbitals on a layer of fluorine atoms parallel to the $xy$ plane for (a) the $\Gamma_{25}'$ and (b) the $\Gamma_{15}$ valence-band states. Each solid dot represents a fluorine atom and the loops are the $p_x$ orbitals.

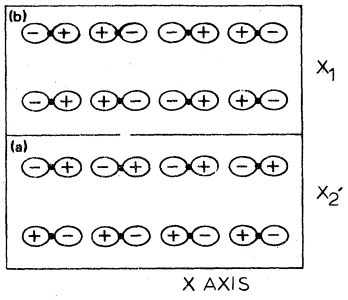


FIG. 3. Schematic diagrams of the $p_x$-type orbitals on a layer of fluorine atoms parallel to the $xy$ plane for (a) the $X_2'$ and (b) the $X_1$ valence-band states. Each solid dot represents a fluorine atom and the loops are the $p_x$ orbitals.

### B. Conduction bands

In Fig. 1 is shown the CB obtained by using the 77-function basis set. The lowest CB state is at $\Gamma$; this gives a direct band gap of 10.0 eV at $\Gamma$. The top of VB however is at $X$, thus the indirect gap is 9.8 eV. The $\Gamma_1$ state of the CB is composed of $s$ orbitals of Ca and F. The Ca contribution to $\Gamma_1$ consists of mainly the $s$-type single Gaussians with small components of $3s$, $2s$, and $1s$, and therefore can be viewed qualitatively as a modified $4s$ state. The $\Gamma_{12}$ and $\Gamma_{25}'$ states result directly from the Ca $3d$ states, containing no Ca $s$ and $p$ components. Furthermore $\Gamma_{12}$ does not mix with any $s$- and $p$-type orbitals on the F sites, and the F-$3d$ admixture is very small. This makes $\Gamma_{12}$ almost a pure Ca $3d$ state. For $\Gamma_{25}'$ mixing with F $p$ orbitals is allowed. Here we have $\Gamma_{12}$ below $\Gamma_{25}'$ whereas the reverse order was found in CaO. The reason for this is that a Ca atom in $CaF_2$ is surrounded by eight F atoms at the corner of a cube (cubic coordination), whereas the Ca atoms in CaO are octahedrally coordinated (six F atoms on the center of each face of the cube). It is well known in crystal-field theory that the $e$-$t_2$ ($\Gamma_{12}$

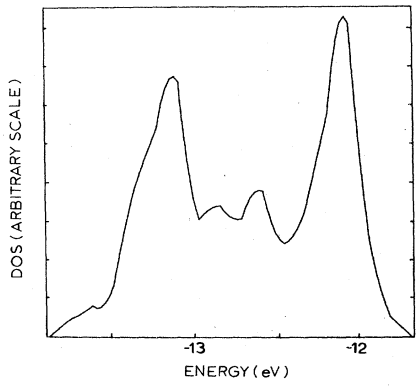


FIG. 4. Density of states of the valence bands of $CaF_2$.

$-\Gamma'_{15}$) splitting of a $3d$ state is reversed from a cubic to an octahedral coordination.[16] Although a point-charge model is generally invoked for an analytic theoretical proof, the $e$-$t_2$ reversal is verified experimentally, even for complex ions with large overlapping between the transition-metal ion and the ligands.[16] The $\Gamma_{15}$ state in the CB is composed of $p$-type orbitals of both Ca and F. As we move away from the $\Gamma$ point, the $d$ orbitals are no longer well segregated from the others. To delineate the effects of the $d$ orbitals, we perform a band calculation with all the $d$-type basis functions deleted from the 77-function set, and present the results in Fig. 5. In the absence of the $d$ states, the $\Gamma_1$-$\Delta_1$-$X_1$ branch (CB) ascends monotonically in energy, differing markedly from the one calculated with $d$ orbitals included. The Ca $d$ states not only manifest themselves in $\Gamma_{12}$, $\Gamma'_{15}$, and their associated branches, but also cause serious modification of the lowest part of the CB through their interaction with the Ca $4s$ states. As another test calculation, we retain all the Ca $d$-type basis functions, but delete only the $d$ functions at the F sites. The resulting energies are practically the same as those obtained with the F $d$ functions included for the CB states below $E=2.0$ eV. The relative unimportance of the F $d$ orbitals for the lower part of the CB is understandable because in atomic F the $3d$ state is 16 eV above $2p$.

The DOS for the CB is exhibited in Fig. 6. The large peak (0.4 eV) is due to a band which is rather undispersive over the entire BZ. The flatness of this band along the $L$-$\Gamma$-$X$-$K$-$\Gamma$ lines is evident in Fig. 1. The lower peak at $-0.4$ eV shows some structure and corresponds to a band which is much more dispersive than the one above it. Only some

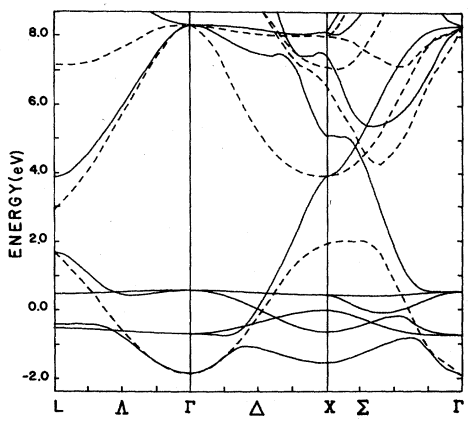


FIG. 5. Conduction bands of $CaF_2$. The solid curves were calculated with the 77-function basis set ($d$ states included) and the dashed curves obtained by deleting all $d$-type basis functions from the 77-function set.

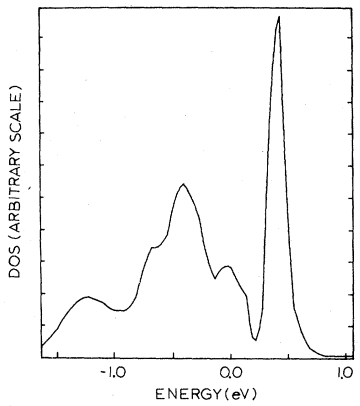


FIG. 6. Density of states of the conduction bands of $CaF_2$.

parts of the BZ contribute to the lower peak. The DOS drops drastically above 0.6 eV, in fact the energy levels concentrate heavily within an energy interval of 1.2 eV in which the Ca $3d$ states play an important role. The abundance of states in that region is further enhanced by the higher multiplicity of the $d$ states (as compared to $s$ and $p$). For the states below $-0.5$ eV, the cation orbitals are largely of $s$ type and the DOS is much lower.

It is interesting to examine the joint density of states between the VB and CB which is displayed in Fig. 7(a). We can explain the positions of the

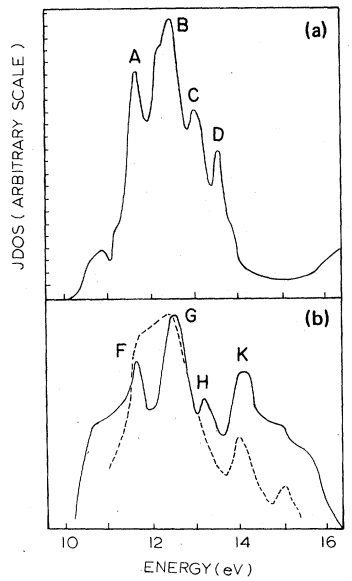


FIG. 7. (a) Joint density of states between the valence and conduction bands of $CaF_2$, (b) experimental reflectance spectrum of Ref. 3 (solid curve), and experimental $\epsilon_2$ curve of Ref. 4 (dashed curve). Both curves have been shifted downward by 1.5 eV to compensate for the difference between the experimental and theoretical values of the band gap.

four peaks (marked as $A$, $B$, $C$, and $D$ at 11.7, 12.4, 13.0, and 13.5 eV, respectively) easily by referring to the individual DOS of the VB and Cb in Figs. 4 and 6. The energy increments from the two major peaks in the DOS of the VB (at −12.1 and −13.1 eV) to the two peaks of the CB (at −0.41 and 0.41 eV) are 11.7, 12.5, 12.7, and 13.5 eV, which are very close to the energies of peaks $A$, $B$, and $D$ in Fig. 7. To account for peak $C$ we note that the energy differences between the prominent peak of the CB (0.41 eV) and the two secondary peaks of the VB (−12.8 and −12.6 eV) are 13.2 and 13.0 eV.

## IV. COMPARISON WITH OTHER WORKS AND EXPERIMENTS

### A. Valence bands

Calculations of the VB structure of $CaF_2$ have been reported by Albert, Jouanin, and Gout.[6] They used the LCAO method with a basis set consisting of the Bloch sums of all the occupied states. Their crystal potential was obtained by making the OAP approximation with the exchange part slightly modified as explained in Ref. 6. In their later work[7] an additional approximation of "spherical averaging" was introduced to calculate the Hamiltonian matrix elements, but the resulting VB structure does not differ significantly from the earlier results. Since they did not carry out the band solutions to self-consistency, the band gap obtained from the OAP model with the exchange parameter $\alpha=1$ is larger than the experimental value. Therefore they chose $\alpha=0.795$ in order to match the calculated band gap with the experimental value 12.1 eV.

In spite of the difference in crystal potential, our VB structure shows the same general features as does the one of Ref. 7. The latter also has both the upper and lower boundary of the VB at $X$. Our VB width of 2.0 eV lies between the values of Refs. 6 and 7 (1.6 and 2.7 eV). Poole *et al.* reported photoemission measurements for $CaF_2$ and obtained for the VB a full width at half-maximum (FWHM) as 3.0 eV and a total width of 4.8 eV. Our calculated FWHM for the VB DOS is 1.6 eV. Also, the shape of the photoemission spectrum is quite different from our DOS curve. Another experimental measurement, attributed to Bremser, gives 1.2 eV.[17] In view of the variance between the two sets of experimental data, definitive comparison between theory and experiment cannot be made at this stage. However, as will be seen in Sec. IV C, there is an indication that the calculated bandwidth of 2.0 eV may be slightly too small. Our calculation places the top of the VB 11.7 eV below the vacuum level which compares satisfactorily with a photoemission onset of about 10.5 eV deduced from the experiment of Poole *et al.*

### B. X-ray structure factors

Measurements of x-ray scattering structure factors have been reported by Togawa[18] and by Weiss, Witte, and Wölfel.[19] Maslen[20] analyzed these experimental data and compared them with theoretical values calculated by approximating the crystal charge distribution as (i) a lattice sum of the free-ion Hartree-Fock charge densities, (ii) a lattice sum of the neutral-atom Hartree-Fock charge densities, and (iii) a lattice sum of charge densities of the "crystal ions" which are modified versions of the free ions with allowance for the effect of the Madelung potential in a special way. Of these three approximations, Maslen obtained the best fit with experiment using the free-ion superposition model.

From the SCF crystal charge density which we determine in this band calculation, one can calculate the theoretical structure factors without resorting to the approximate models mentioned above. Following the notation of Ref. 20, we write the structure factor for the reciprocal-lattice vector characterized by $(hkl)$ as

$$F(hkl)=(f_0+\Delta f'+i\Delta f'')_{\mathrm{Ca}}\exp(-B_{\mathrm{Ca}}\lambda^{-2}\sin^2\theta) + \sigma(f_0+\Delta f'+i\Delta f'')_{\mathrm{F}}\exp(-B_{\mathrm{F}}\lambda^{-2}\sin^2\theta), \tag{13}$$

where $f_0$ stands for the atomic form factors, $\Delta f$ and $\Delta f'$ are the real and imaginary parts of the anomalous dispersion corrections when the x-ray wavelength ($\lambda$) is not very small, $B_{\mathrm{Ca}}$ and $B_{\mathrm{F}}$ are crystallographic $B$ factors for temperature correction, $\theta$ is the angle of reflection, and $\sigma$ is equal to $2\cos(\vec{K}\cdot\vec{t}_1)$; i.e.,

$$\sigma=\begin{cases}2 \text{ for } hkl=220,\ 400,\ 422, \text{ etc.}\\ 0 \text{ for } hkl=111,\ 311,\ 331, \text{ etc.}\\ -2 \text{ for } hkl=200,\ 222,\ 420, \text{ etc.}\end{cases} \tag{14}$$

To calculate $f_0$ we decompose the SCF crystal electron density (determined from Sec. II) into a lattice superposition by curve-fit as

$$\rho^{\mathrm{SCF}}_{\mathrm{cry}}(r)=\sum_\nu[\rho^S_c(\vec{r}-\vec{R}_\nu)+\rho^S_a(\vec{r}-\vec{R}_\nu-\vec{t}_1) + \rho^S_a(\vec{r}-\vec{R}_\nu-\vec{t}_2)]. \tag{15}$$

The form factors of $\rho^S_c(r)$ and $\rho^S_a(r)$ yield, respectively, $(f_0)_{\mathrm{Ca}}$ and $(f_0)_{\mathrm{F}}$. Two sets of $\Delta f'$ and $\Delta f''$ corresponding to the two wavelengths used in the experimental works have been given in Ref. 20, and the $B$ factors in Refs. 18 and 19. Togawa

reported only scattering data for the cases of $\sigma=2$ and $\sigma=0$ in Eq. (14), whereas the measurements of Weiss *et al.* cover all three kinds ($\sigma=0$, $\pm2$). In this paper we adopt, for comparison with the theoretical values, the experimental structure factors of Togawa for $\sigma=2,0$ and those of Weiss *et al.* for $\sigma=-2$ which are listed in Table II. Included for comparison are the theoretical values calculated from Eq. (13) with the values of $\Delta f'$ and $\Delta f''$ appropriate for the wavelengths used in the experimental measurements. The $B$ factors are taken as 0.63 and 0.74 Å$^2$ for Ca and F, respectively, in accordance with Ref. 18. We notice that the structure factors measured by Togawa are all somewhat larger than the theoretical values. This pattern of deviation is understandable since the experimental values do not result from absolute measurements. Instead, relative values of structure factors were determined experimentally and brought to absolute scale by comparing them with the theoretical form factors of the *free ions*. The one-sided discrepancy may be attributed to that choice of normalization factor which is based on a free-ion approximation. If we renormalize Togawa's data by a multiplicative factor of 1.03 as shown in the last column of Table I, the agreement between theory and experiment becomes very good with an average discrepancy of 1.5%. As to the case of $\sigma=-2$, the theoretical values are in much poorer accord with the experimental data of Weiss *et al.* Of course, these structure factors are weak and subject to larger percentage experimental errors. Also from the theoretical standpoint, the structure factors for $\sigma=-2$ involve a substantial cancellation between the contributions from Ca and from F as shown in Eq. (13). Nevertheless, the discrepancy for the lower members of this series is larger than what we would expect. It should be mentioned that a better agreement is shown by Maslen in Ref. 20 between the experimental structure factors and his theoretical values based on a free-ion model. This is because Maslen introduced an adjustable multiplicative factor for renormalizing each set of experimental data, as well as treating the $B$ factors as adjustable parameters to give the best fit.

TABLE II. Comparison between the theoretical and experimental x-ray structure factors.

| $hkl$ | $\sigma$ | $\lvert F(hkl)\rvert_{\text{expt}}$ | $\lvert F(hkl)\rvert_{\text{theor}}$ | $1.03\times\lvert F(hkl)\rvert_{\text{expt}}$ |
|---|---|---|---|---|
| 111 | 0 | 15.54 | 15.80 | 16.00 |
| 311 | 0 | 11.29 | 11.54 | 11.62 |
| 331 | 0 | 9.08 | 9.27 | 9.35 |
| 511, 333 | 0 | 7.66 | 7.90 | 7.89 |
| 531 | 0 | 6.95 | 6.99 | 7.16 |
| 533 | 0 | 6.18 | 6.32 | 6.37 |
| 220 | 2 | 23.61 | 24.51 | 24.32 |
| 400 | 2 | 16.89 | 18.02 | 17.40 |
| 422 | 2 | 13.75 | 14.39 | 14.16 |
| 440 | 2 | 11.42 | 12.12 | 11.76 |
| 620 | 2 | 10.19 | 10.56 | 10.50 |
| 200 | −2 | 0.71 | 0.34 | |
| 222 | −2 | 2.12 | 1.52 | |
| 420 | −2 | 2.58 | 2.03 | |
| 600, 442 | −2 | 2.72 | 2.40 | |
| 622 | −2 | 2.72 | 2.42 | |

### C. Conduction bands

The theoretical works of Albert *et al.*[6,7] extend also to the conduction states. In their first paper they obtain the CB by means of the method of OPW in place of the LCAO method which they used for the VB. These authors examined the convergence of the OPW expansion at $\Gamma$, and indicated that full convergence for the $d$ states ($\Gamma_{12}$ and $\Gamma'_{25}$) would require a basis set larger than the 160-OPW set that they employed. Comparison of their CB with our Fig. 1 indeed shows that their $\Gamma_{12}$ and $\Gamma'_{25}$ states are considerably higher than ours. Their $\Gamma_1$-$\Delta_1$-$X_1$ branch rises monotonically and differs significantly from ours. This may be explained on the ground that their $d$ states are well above the $s$ states, causing much less distortion on the bottom $s$-type band. The relative order of $\Gamma_{12}$ and $\Gamma'_{25}$ in their results, however, is the same as ours. As indicated before, the calculation of Albert *et al.* is not an SCF one. They used an OAP-type potential and chose $\alpha=0.795$ in order to match the calculated band gap to the experimental value of 12.1 eV. In our calculation we retain the full Slater exchange ($\alpha=1$) and obtain a band gap (direct) of 10.0 eV with an SCF calculation.

Albert *et al.* subsequently replaced the OPW method by a pseudopotential procedure to obtain the CB structure. The cation $d$ states were still found to be too high ($\Gamma'_{25}$ being 10 eV above $\Gamma_1$). They attributed this to the inadequacy of the pseudopotential method in its standard form as applied to $d$ bands. As a remedy they add a partial $d$-wave potential well to the standard potential. This substantially pushes the $d$ states down so that $\Gamma'_{25}$ now is 4.3 eV above $\Gamma_1$. However, in both of these pseudopotential calculations, the order of $\Gamma'_{25}$ and $\Gamma_{12}$ is reversed as compared to the earlier OPW results. In view of the empirical nature of the calculations reported in Ref. 7, it is difficult to correlate their results with ours.

Optical experiments have been reported by several research groups.[1-4] A sharp peak (11.2 eV) at the low-energy edge was observed in the reflectance spectra[3] and is interpreted as excitons

associated with the fundamental direct gap. Following this peak is a shoulder at 12.1 eV which was assigned by Rubloff[3] as the $\Gamma_{15} \rightarrow \Gamma_1$ interband transition, and this value was taken as the band gap. It is appreciably larger than our calculated value of 10.0 eV. However, referring to the theoretical JDOS shown in Fig. 7, the first shoulder occurs at 10.7 eV even though the band gap is 10.0 eV. Thus the experimental band gap may be somewhat lower than 12.1 eV, for example, as low as 11.5 eV. A similar situation exists for CaO in which an SCF calculation with $\alpha = 1$ gives a band gap 14% lower than the experimental value.

There is some disagreement in the literature regarding the interpretation of the structures in the observed spectra. This is mostly due to the different assumptions on the CB structure which were made in order to analyze the optical data. For instance, a model band structure for $CaF_2$ similar to that of KCl was taken as a reference point in Ref. 3, whereas Frandon, Lahaye, and Pradel assumed that the lowest CB state is of $X_3$ symmetry. With a one-electron band description we are not able to study exciton effects, but a comparison of our calculated JDOS with the experimental optical data may provide some information concerning the interband transitions. Because the calculated band gap is smaller than the experimental value, it is more instructive to compare the peak positions relative to the onset rather than their absolute energies. This can be done by shifting the energy scale of the experimental spectra by the difference between the experimental and theoretical band gap. Since we have reasons to believe the experimental band gap to be somewhat less than 12.1 eV, we apply a shift of 1.5 eV to the $\epsilon_2$ curve of Frandon *et al.* and to Rubloff's reflectance spectra and include them in Fig. 7(b). Here we delete the leading exciton peak from the experimental data since there is no counterpart in the JDOS curve. We can see considerable resemblance between the JDOS and optical data, particularly the double-peak feature present both in theory ($A$,$B$) and experiment ($F$,$G$). Since peak $H$ observed in the reflectance spectrum is very temperature dependent and does not appear in the $\epsilon_2$ curve of Frandon *et al.*, it may not correspond to an interband transition in spite of its close proximity to peak $C$ in the JDOS. On the other hand, peak $K$ is found in both the reflectance and $\epsilon_2$ spectra, but occurs at a somewhat higher energy than JDOS peaks $C$ and $D$. As we have remarked in Sec. III B, peaks $A$ and $B$ in Fig. 7(a) arise from transitions from the top of the VB to the two groups of CB states which correspond to the two prominent peaks in the DOS (Fig. 6), whereas peaks $C$ and $D$ originate from the lower part of the VB. A possible explanation of the displacement of peak $K$ from $C$ and $D$ in Fig. 7 is that the calculated VB may be slightly too narrow, for if the bottom of the VB were shifted downward by a few tenths of an eV, peaks C and $D$ would move closer to peak $K$ while leaving the positions of peaks $A$ and $B$ unchanged.

It should be mentioned that Rubloff interpreted peak $F$ as excitonic based on analogy to $KCl$, and Frandon *et al.* attributed both $F$ and $G$ to excitons. The results of our calculation favor an interpretation of these peaks as interband transitions. In fact the occurrence of the dominant structure around $F$ and $G$ in the optical data within a few eV to the onset can be understood easily. The first excited state of the free $Ca^+$ ion is $3d$ which lies 1.7 eV above the $4s$ ground state,[21] thus one expects the crystalline $3d$-like levels to be a few eV higher than the threshold of the CB. For the specific case of $CaF_2$, the $\Gamma_{12}$ state is 1.2 eV above the CB edge and the majority of the $3d$-like states are within an energy range of 1.5 eV, where the DOS is high because of the five-fold multiplicity of $d$ states. The density becomes much smaller on either side of this range in which $s$ and $p$ states prevail. With a narrow VB, this means that the major part of the VB-CB transitions must take place at energies only a few eV higher than the band-gap energy.

One significant difference between our results and the earlier band models adopted for interpreting optical experiments concerns the relative location of some $d$-type levels. Of the $\Gamma'_{25}$ and $\Gamma_{12}$ components of the Ca $3d$ CB states, Rubloff assumed the $\Gamma'_{25}$ to be the lower one in analogy to KCl. Along the $\Delta$ line $\Gamma'_{25}$ splits into a nondegenerate and a doubly degenerate level, and the lowest level of the CB at $X$ was assumed by Rubloff to be $X_3$ which involves the $d_{yz}$ orbital of Ca. Frandon *et al.* further assumed the $X_3$ state to be the bottom of the CB (which is the case for CaO). However, $CaF_2$ differs from KCl and CaO in that the cation coordination is of cubic geometry (eight nearest neighbors) for $CaF_2$ but octahedral (six nearest neighbors) for KCl and CaO. As discussed in Sec. III B, this leads to a reversal of the $\Gamma'_{25}$-$\Gamma_{12}$ ordering. With $\Gamma'_{25}$ being the upper one of the Ca $3d$ levels, it lies sufficiently high in the CB so that the entire $\Gamma'_{25}$-$\Delta'_2$-$X_3$ branch is well above the CB boundary (see Fig. 1). In fact our calculation places the bottom of the CB at $\Gamma_1$. Even at the $X$ point the lowest CB state is $X_1$ rather than $X_3$.

A comprehensive analysis of the experimental $\epsilon_2$ data in reference to our band calculation is somewhat premature at this stage, as we have not taken into account the effect of the transition-

moment matrix elements. Also it is an oversimplification to adopt a rigid shift of the CB with respect to the VB (to compensate for the 1.5-eV difference between the theoretical and experimental band gap) in order to correlate the calculated optical transitions with experiments. An obvious direction for a more refined theoretical treatment is to improve the exchange-correlation potential so as to yield a better band gap. Once a good agreement with experiment for the band gap is achieved, one can calculate $\epsilon_2$ and make a detailed comparison with optical data. Such a program is beyond the scope of this paper. Nevertheless, we see a good accord between our calculated JDOS and the optical experiments in their general features, and much of these features can be understood qualitatively from simple considerations based mostly on the nature of the $d$-type CB states.

## V. DISCUSSION AND CONCLUSIONS

By performing a first-principles Hartree-Fock-Slater SCF calculation for the electronic states of the $CaF_2$, we are able to study theoretically the ground-state and optical properties of this crystal. The theoretical x-ray structure factors are in very good agreement with the scattering experiment of Togawa. The very weak structure factors measured by Weiss, Witte, and Wölfel, however, differ substantially from our values. The calculated energy band gap is somewhat smaller than the experimental value. When the exchange parameter $\alpha$ is taken as unity, the initial OAC (or OAP) approximation for the crystal potential leads to a band gap higher than the experimental value, but the gap drops below it when self-consistency is reached. This appears to be a rather common feature for highly ionic crystals as found in the cases of LiF,[12] LiCl,[22] CaO,[13] and MgO.[23] The use of $\alpha = \frac{2}{3}$ may be better suited for ground-state properties, but would give an even smaller band gap. It should be worthwhile to explore other forms of exchange-correlation potential with the hope of improving the calculated band gap.

The LCAO wave functions allow us to delineate clearly the atomic characteristic of the constituents. This is especially important for ionic crystals, as it provides a realistic picture for qualitative description. For instance, the VB states are found to be composed almost exclusively of F $2p$ orbitals and the lowest part of the CB originates from the $4s$ orbital of the cation. The Ca $3d$ orbitals play a dominant role in the energy range of 1.2–3.0 eV above the threshold of the CB, and are responsible for the large amplitude observed in optical experiments at the corresponding photonenergies.

## ACKNOWLEDGMENT

The authors wish to acknowledge support by the National Science Foundation.

## APPENDIX

The initial crystal charge density (zeroth order) for the SCF iteration is taken as a superposition of the free-atom electron densities of the $Ca^{++}$ and $F^-$ as indicated in Eq. (5); i.e.,

$$\rho_{\rm cry}^{(0)}(\vec{r}) = \sum_{\nu} [\rho_{Ca^{++}}(\vec{r} - \vec{R}_\nu) + \rho_{F^-}(\vec{r} - \vec{t}_1 - \vec{R}_\nu) + \rho_{F^-}(\vec{r} - \vec{t}_2 - \vec{R}_\nu)] . \quad \text{(A1)}$$

Correspondingly the Coulomb part of the crystal potential is a superposition of the individual atomiclike components $[V_i(\vec{r})]_C$ where $i$ designates $Ca^{++}$ or $F^-$, and the subscript $C$ stands for Coulomb interaction. To obtain $V_i$ we determine the electrostatic potential, called $U_i$, due to $\rho_i$ and combine it with the potential of the nucleus as

$$[V_i(\vec{r})]_C = Z_i/r + U_i(\vec{r}) . \quad \text{(A2)}$$

We artificially decompose $\rho_i(\vec{r})$ into

$$\rho_i(\vec{r}) = \rho_i'(\vec{r}) + \rho_i''(\vec{r}) , \quad \text{(A3)}$$

where $\rho_i'(\vec{r})$ is of sufficiently short range that there is virtually no overlap between two $\rho_i'$ functions centered at nearest-neighbor sites. It includes the core charge and part of the valence charge. If we denote the amount of charge (absolute value) contained in $\rho_i'$ by $Z_i'$, then $V_i$ can likewise be divided into a nonoverlapping and an overlapping component:

$$[V_i(\vec{r})]_C = [V_i'(\vec{r})]_C + [V_i''(\vec{r})]_C , \quad \text{(A4)}$$

$$[V_i'(\vec{r})]_C = Z_i'/r + U_i'(\vec{r}) , \quad \text{(A5)}$$

$$[V_i''(\vec{r})]_C = (Z_i - Z_i')/r + U_i''(\vec{r}) , \quad \text{(A6)}$$

where $U'$ and $U''$ are the electrostatic potentials associated with $\rho'$ and $\rho''$, respectively. The same kind of partition also applies to the crystal Coulomb potentials so that

$$[V_{\rm cry}(\vec{r})]_C = [V_{\rm cry}'(\vec{r})]_C + [V_{\rm cry}''(\vec{r})]_C , \quad \text{(A7)}$$

where $[V_{\rm cry}'(\vec{r})]_C$ and $[V_{\rm cry}''(\vec{r})]_C$ are generated by a lattice summation of $[V_i'(\vec{r})]_C$ and $[V_i''(\vec{r})]_C$, respectively. Matrix elements of $[V_{\rm cry}'(\vec{r})]_C$ are computed by integration in the direct space, whereas $[V_{\rm cry}''(\vec{r})]_C$ is handled by a Fourier expansion similar to Eq. (11). With the SCF scheme we obtained the values of the first-order charge density $\rho_{\rm cry}^{(1)}(\vec{r})$ at 353 nonequivalent points. Instead of fitting $\rho_{\rm cry}^{(1)}(\vec{r})$ to a superposition of localized functions as indicated in Eq. (12), we have found it more expedient to subtract $\rho'(\vec{r})$ around each site from $\rho_{\rm cry}^{(1)}$, i.e.,

$$\Delta\rho_{\rm cry}^{(1)}(\vec{r}) = \rho_{\rm cry}^{(1)}(\vec{r}) - \sum_{\nu} [\rho'_{\rm Ca}(\vec{r} - \vec{R}_\nu) + \rho'_{\rm F}(\vec{r} - \vec{R}_\nu - \vec{t}_1) + \rho'_{\rm F}(\vec{r} - \vec{R}_\nu - \vec{t}_2)] ,$$

and fit $\Delta_{\rm cry}^{(1)}(\vec{r})$, rather than $\rho_{\rm cry}^{(1)}(\vec{r})$, to a superposition form. Compared to $\rho_{\rm cry}^{(1)}(\vec{r})$ itself, $\Delta\rho_{\rm cry}^{(1)}(\vec{r})$ is much smoother and easier to fit because the troublesome core charge-density spikes are eliminated. The result of this fit gives the first-iteration version of $\rho_i''(\vec{r})$ which in turn leads to the Fourier coefficients and therefore the matrix elements of an improved $[V''_{\rm cry}(\vec{r})]_C$. Since $\rho_i'(\vec{r})$ is kept fixed and not allowed to change during each iteration, the matrix elements of $[V'_{\rm cry}(\vec{r})]_C$ need not be recalculated. For the exchange potential, $[\rho_{\rm cry}(\vec{r})]^{1/3}$ is much smoother than $\rho_{\rm cry}(\vec{r})$, and we simply perform the lattice-superposition fitting of $[\rho_{\rm cry}(\vec{r})]^{1/3}$ as indicated in Eqs. (7) and (12).


[1] T. Miyata and T. Tomiki, J. Phys. Soc. Jpn. 24, 954 (1968).
[2] G. Stephan, Y. LeCalvez, J. C. Lemonier, and S. Robin, J. Phys. Chem. Solids 30, 601 (1969).
[3] G. W. Rubloff, Phys. Rev. B 5, 662 (1971).
[4] J. Frandon, B. Lahaye, and F. Pradel, Phys. Status Solidi B 53, 565 (1972).
[5] R. T. Pool, J. Szajman, R. C. G. Leckey, J. G. Jenkin, and J. Liesegang, Phys. Rev. B 12, 5872 (1975).
[6] J. P. Albert, C. Jouanin, and C. Gout, Phys. Rev. B 16, 925 (1977).
[7] J. P. Albert, C. Jouanin, and C. Gout, Phys. Rev. B 16, 4619 (1977).
[8] J. E. Simmons, C. C. Lin, D. F. Fouquet, E. E. Lafon, and R. C. Chaney, J. Phys. C 8, 1549 (1975).
[9] E. E. Lafon and C. C. Lin, Phys. Rev. 152, 579 (1966).
[10] R. C. Chaney, T. K. Tung, C. C. Lin, E. E. Lafon, J. Chem. Phys. 52, 361 (1970).
[11] F. Herman and S. Skillman, *Atomic Structure Calculations* (Prentice-Hall, Englewood Cliffs, N. J., 1963).
[12] R. C. Chaney, E. E. Lafon, and C. C. Lin, Phys. Rev. B 4, 2734 (1971).
[13] U. Seth and R. C. Chaney, Phys. Rev. B 12, 5923 (1975).
[14] R. Heaton and E. Lafon, Phys. Rev. B 17, 1958 (1978).
[15] R. S. Mulliken, J. Chem. Phys. 23, 1833 (1955); 23, 1841 (1955).
[16] C. J. Ballhausen, *Introduction to Ligand Field Theory* (McGraw-Hill, New York, 1962).
[17] This was cited in Ref. 7.
[18] S. Togawa, J. Phys. Soc. Jpn. 19, 1696 (1964).
[19] A. Weiss, H. Witte, and E. Wölfel, Z. Physik. Chem. Neue Folge 10, 98 (1957); H. Witte and E. Wölfel, Rev. Mod. Phys. 30, 51 (1958).
[20] V. W. Maslen, Proc. Phys. Soc. London 91, 466 (1967).
[21] C. E. Moore, Natl. Bur. Std. (U.S.) Circ. No. 467, 246 (1949).
[22] J. G. Harrison and C. C. Lin (unpublished).
[23] R. C. Chaney, private communication.